



OPEN

Fe₃O₄@nano-almondshell/Si(CH₂)₃/2-(1-piperaziny) ethylamine as an effective magnetite almond shell-based nanocatalyst for the synthesis of dihydropyrano[3,2-c]chromene and tetrahydrobenzo[*b*]pyran derivatives

Dina Mallah¹, Bi Bi Fatemeh Mirjalili^{1✉} & Abdolhamid Bamoniri²

The preparation and design of nano-catalysts based on magnetic biopolymers as green and biocompatible nano-catalysts have made many advances. This paper deals with the preparation of magnetite biopolymer-based Brønsted base nano-catalyst from a nano-almond (*Prunus dulcis*) shell. This magnetite biopolymer-based nano-catalyst was obtained through a simple process based on the core-shelling of nano-almond shell and Fe₃O₄ NPs and then the immobilization of 3-chloropropyltrimethoxysilane as linker and 2-aminoethylpiperazine as a basic section. Structural and morphological analysis of this magnetite biopolymer-based nano-catalyst were done using Fourier transform infrared spectroscopy, field emission scanning electron microscopy, X-ray diffraction, Thermogravimetric analysis, Vibrating sample magnetization, Energy-dispersive X-ray spectroscopy, Brunauer–Emmett–Teller, and Transmission electron microscopy techniques. The performance of the synthesized Fe₃O₄@nano-almondshell/Si(CH₂)₃/2-(1-piperaziny)ethylamine as a novel magnetite biopolymer-based nano-catalyst for the synthesis of dihydropyrano[3,2-c]chromene and tetrahydrobenzo[*b*]pyran was investigated and showed excellent efficiency.

In recent years, extensive research has been conducted on new polymer-based nano-catalysts. New polymers known as biopolymers will be synthesized from non-edible and highly available plants as well as agricultural and industrial wastes^{1–3}. In addition, some biopolymers can be obtained from renewable sources. These biopolymers include polysaccharides (cellulose, dextrin, chitosan, etc.), protein polymers (gluten, ovalbumin, soy protein, collagen, etc.), bacterial protein (3-hydroxybutyrate), and other polymers⁴. Among these biopolymers, cellulose, and derivatives become important due to their high flexibility, abundance, chemical inertness, high strength, and ability to modify surface chemistry^{5–8}. The almond (*Prunus dulcis*) shell is a highly efficient biomass shell and is generally disposed of or incinerated as waste, which causes environmental pollution⁹. Almond shells make up about 35–75% of the total weight of the fruit. This volume of the shell has a high practical potential that has attracted a lot of attention in recent years^{10,11}. Senturk et al. used the almond shell as an adsorbent to remove rhodamine dye from aqueous solutions¹². Mohan et al. have prepared magnetically activated carbon from almond shells to remove 2,4,6-trinitrophenol from water¹³. Cellulose is one of the main components of the almond shell, which turns this waste into suitable material for preparing nano-catalysts^{14,15}.

¹Department of Chemistry, College of Science, Yazd University, P.O. Box 89195-741, Yazd, Islamic Republic of Iran. ²Department of Organic Chemistry, Faculty of Chemistry, University of Kashan, Kashan, Islamic Republic of Iran. ✉email: fmirjalili@yazd.ac.ir

Benzopyran or chromene is an organic bicyclic heterocyclic compound consisting of benzene and pyran rings^{16,17}. Chromene derivatives have various biological and medicinal properties and therapeutic applications that have been considered by pharmaceutical and organic chemists¹⁸. Chromenes have shown a variety of biological properties such as antimicrobial¹⁹, antibacterial²⁰, anticancer²¹, anti-HIV²², and sex pheromone²³. Therefore, due to the biological and therapeutic properties and the great importance of chromenes, several pathways for the synthesis of these compounds have been reported, including one-step or multi-step methods²⁴. One of the best attractive methods for the synthesis of chromenes is based on multi-component reactions (MCRs)^{25,26}. Multicomponent reactions are one of the most successful methods in the field of increasing structural diversity and molecular complexity using a simple process. This method, as a developing process for the preparation of organic compounds, allows the development of many chemical compounds, with more structural diversity. Also, these reactions are considered a useful and effective tool for the synthesis of organic compounds and generally show good selectivity along with the reduction of by-products compared to the classical step-by-step preparation^{27,28}. Higher efficiency, simplicity, saving time, and materials are some of the advantages of this category of reaction²⁹. Dihydropyrano[3,2-*c*]chromene and tetrahydrobenzo[*b*]pyran are heterocyclic organic compounds containing oxygen and are very attractive. For this reason, so far, many catalysts including ZnO NPs³⁰, t-ZrO₂ NPs³¹, SB-DABCO@eosin³², Fe₃O₄@GO-NH₂³³, [PEMIM][OH]³⁴, [(EMIM)Ac]³⁵, L-Proline³⁶, Chitosan-ZnO³⁷, CESA³⁸, Glycine³⁹, rGO@Fe₃O₄@ZrCp₂Cl₂⁴⁰, Fe₃O₄@*G.tea*/Cu⁴¹, etc. have been used for the synthesis of this class of compounds.

In this work, Fe₃O₄@nano-almondshell/Si(CH₂)₃/2-(1-piperaziny)ethylamine, abbreviated FNASiPPEA, as magnetite almond shell-based nano-catalyst was prepared and identified using FT-IR, FESEM, XRD, TGA, VSM, EDS-map, BET, TEM techniques, and then use it in the synthesis of the dihydropyrano[3,2-*c*]chromene and tetrahydrobenzo[*b*]pyran under optimized conditions (Fig. 1).

Results and discussions

In this paper, the FNASiPPEA, a magnetite biopolymer-based nano-catalyst, was used as an environmentally friendly basic nano-catalyst for the synthesis of dihydropyrano[3,2-*c*]chromene (DHPC) and tetrahydrobenzo[*b*]pyran (THBP) derivatives through a multicomponent reaction under optimized conditions. The FNASiPPEA was first prepared by preparing Fe₃O₄@nanoalmondshell according to previously reported methods⁴². After

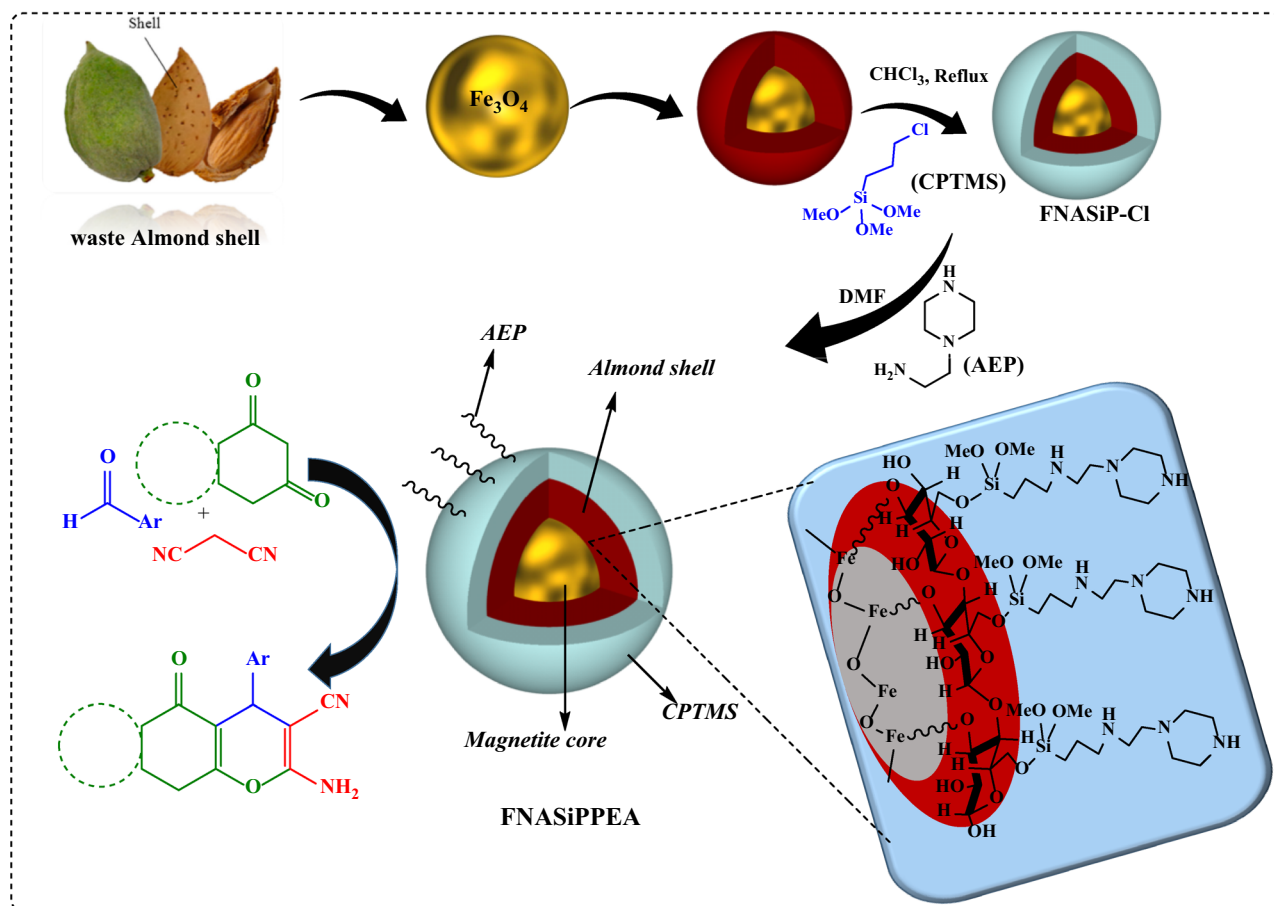


Figure 1. Schematic representation of FNASiPPEA, dihydropyrano[3,2-*c*]chromene, and tetrahydrobenzo[*b*]pyran.

that, FNASiPPEA was prepared by immobilization of 3-chloropropyltrimethoxysilane (CPTMS) and finally 2-aminoethylpiperazine (AEP) (as a base agent) on the surface of the nano-catalyst.

FT-IR of FNASiPPEA. FT-IR spectra of Fe_3O_4 @nanoalmondshell, AEP, and FNASiPPEA are shown in Fig. 2. FT-IR spectrum of nano-almondshell (Fig. 2a) shows distinct peaks at 3428 cm^{-1} , 2920 cm^{-1} , and 1122 cm^{-1} , which are related to O–H, C–H, and C–O vibrational stretching, respectively. In the FNASiPPEA spectrum (Fig. 2c), a distinct peak at 588 cm^{-1} is attributed to the Fe–O stretching vibration. Also, the broad peak at the range of 3400 cm^{-1} is attributed to the stretching vibration of N–H, which overlaps with the stretching vibration of the O–H group. CPTMS immobilization on Fe_3O_4 @nanoalmondshell is confirmed by a characteristic peak at 1111 cm^{-1} , which corresponds to the Si–O stretching vibration. The characteristic peak at 1451 cm^{-1} is related to C–N stretching vibration.

FESEM and TEM of FNASiPPEA. The surface morphology and detailed structure of the FNASiPPEA nano-catalyst were investigated using FESEM (Fig. 3). Figures 3a and b show the average particle size of the catalyst (11–43 nm) which appeared as nanospheres with pseudo-spherical morphology. The intrinsic structure was characterized using TEM measurements (Fig. 3c) which show core–shell nanoparticles.

PXRD (Powder X-ray diffraction) of FNASiPPEA. Figure 4 shows the XRD patterns of Fe_3O_4 NPs and magnetite biopolymer-based FNASiPPEA nanoparticles. All the diffraction peaks appearing at $2\theta = 31^\circ$, 35° , 43° , 54° , 57° , and 63° in the spectrum (4a) can be indexed as centered cubic Fe_3O_4 , which agrees well with the reported data correspond⁴³. In the XRD pattern (4b), a new peak appears at $2\theta = 23^\circ$ and a broad peak at $2\theta = 20\text{--}30^\circ$, which is due to the presence of nano-almondshell and amorphous silica, respectively.

TGA of FNASiPPEA. Figure 5 shows the TGA and DTA curves of magnetite FNASiPPEA. The nano-catalyst shows a small initial mass reduction at a temperature lower than 100°C due to the removal of absorbed water and other organic solvents. At temperatures higher than 100°C , ($180\text{--}370^\circ\text{C}$) the highest weight loss is observed in the TGA curve, which was probably due to the decomposition of nano-almondshell and organic parts (amine groups and methoxy groups) from the catalyst.

VSM of FNASiPPEA. The magnetic properties of the FNASiPPEA were evaluated in Fig. 6. The magnetic curve shows no remanence and coercivity, indicating the nanocatalyst's superparamagnetic behavior. The saturation magnetization value of FNASiPPEA (33 emu/g) is lower than that of Fe_3O_4 (47 emu/g). The low magnetization of the catalyst is attributed to the non-magnetic functionalized nano-almond shell coating on Fe_3O_4 NPs. However, the magnetic susceptibility of FNASiPPEA is strong enough to be separable by an external magnet from the reaction medium.

EDX and EDS-map of FNASiPPEA. The elemental composition of the FNASiPPEA nano-catalyst was determined by EDX. As shown in Fig. 7, Fe, O, C, Si, and N signals are related to respectively, Fe_3O_4 , and functionalized nano-almondshell, which appears in the EDX spectrum. The percentage composition of Fe, C, O, N, Cl, and Si elements is 30.39, 25.50, 15.39, 19.55, 9.08, and 0.48% respectively. According to the results of the EDS-mapping analysis Fig. 8, the distribution of these elements is homogeneously on the surface of the nano-catalyst.

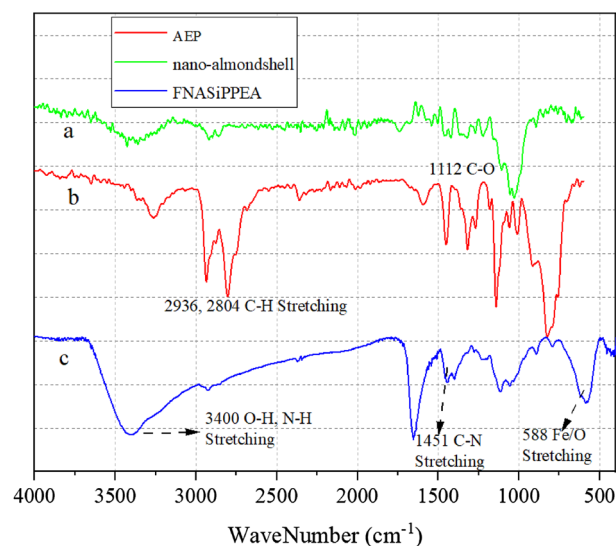


Figure 2. FT-IR spectra of (a) nano-almond shell, (b) AEP, and (c) FNASiPPEA.

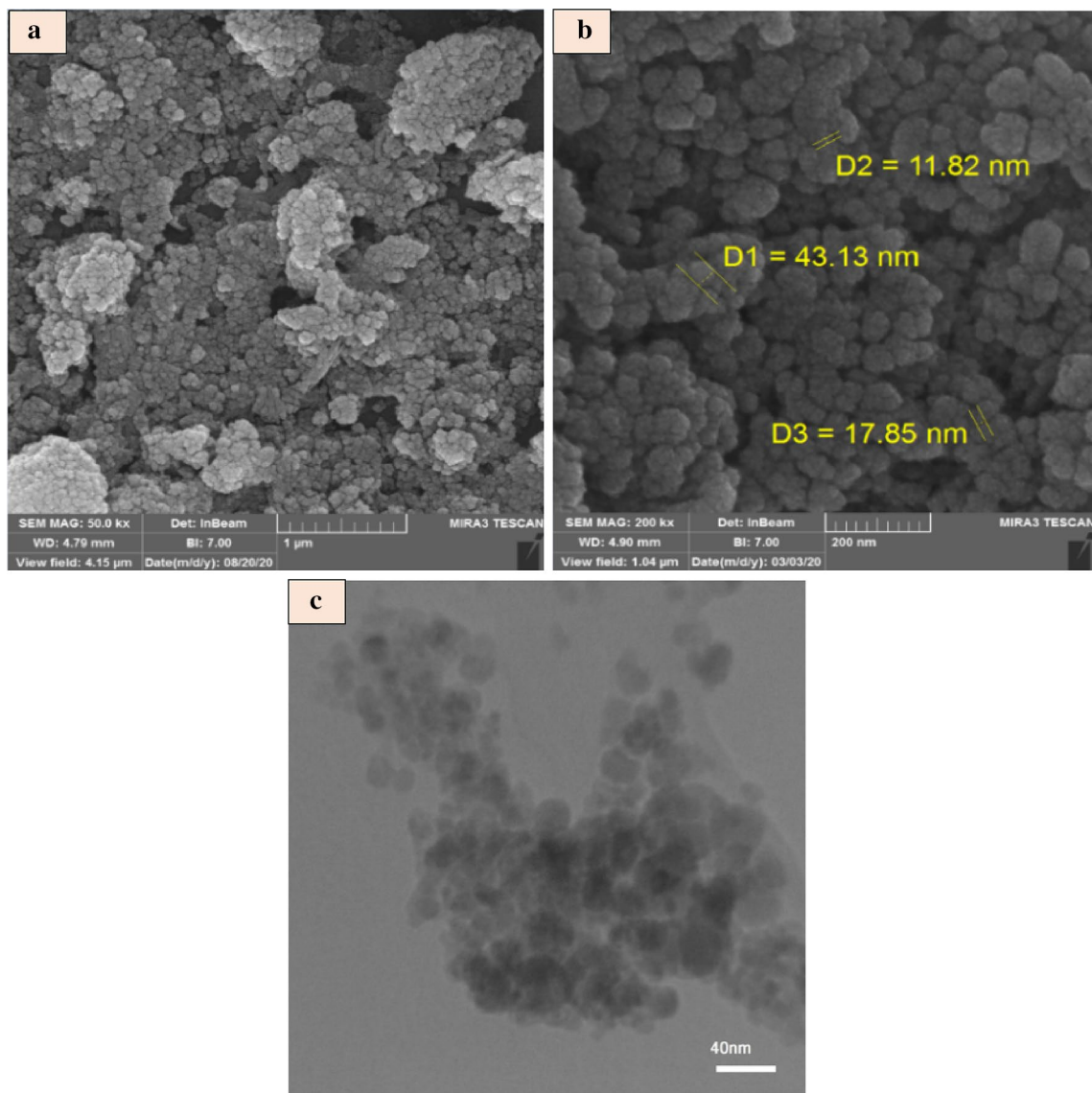


Figure 3. FESEM images of FNASiPPEA (a and b), and (c) TEM of FNASiPPEA.

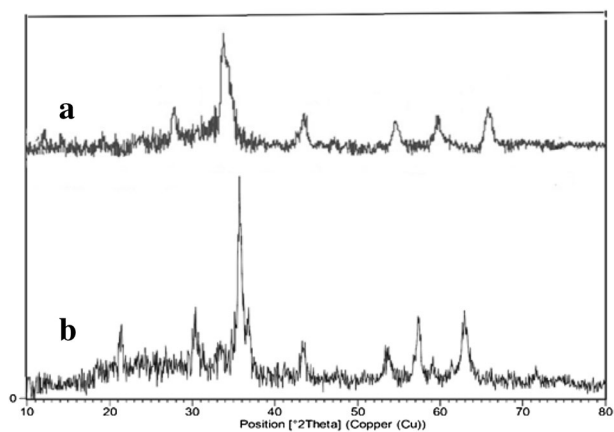


Figure 4. XRD patterns of (a) Fe₃O₄ NPs, and (b) FNASiPPEA.

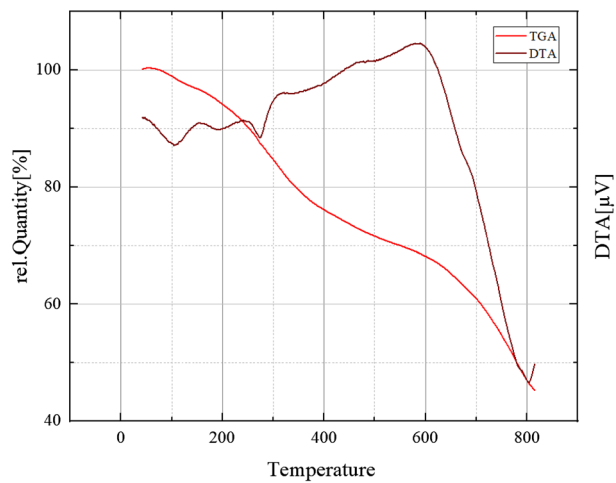


Figure 5. TGA/DTA curves of FNASiPPEA.

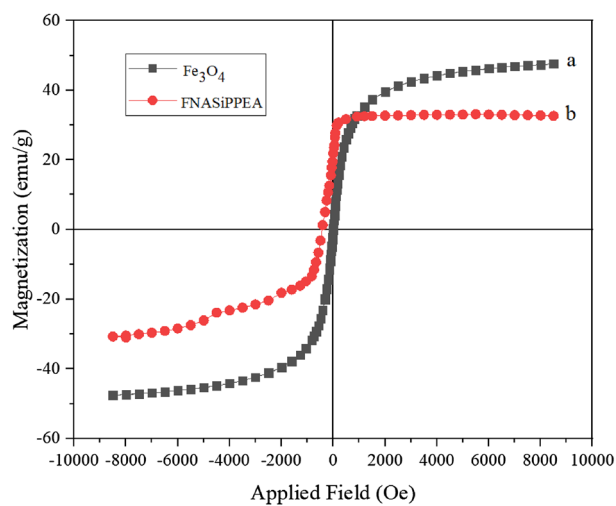


Figure 6. VSM analysis of (a) Fe_3O_4 NPs, (b) FNASiPPEA.

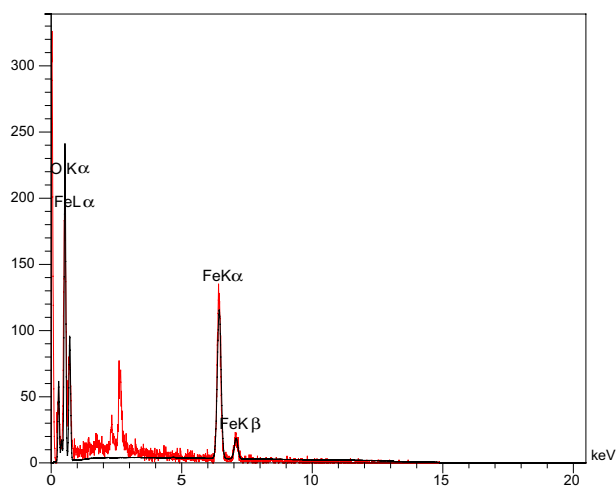


Figure 7. EDS diagram of FNASiPPEA.

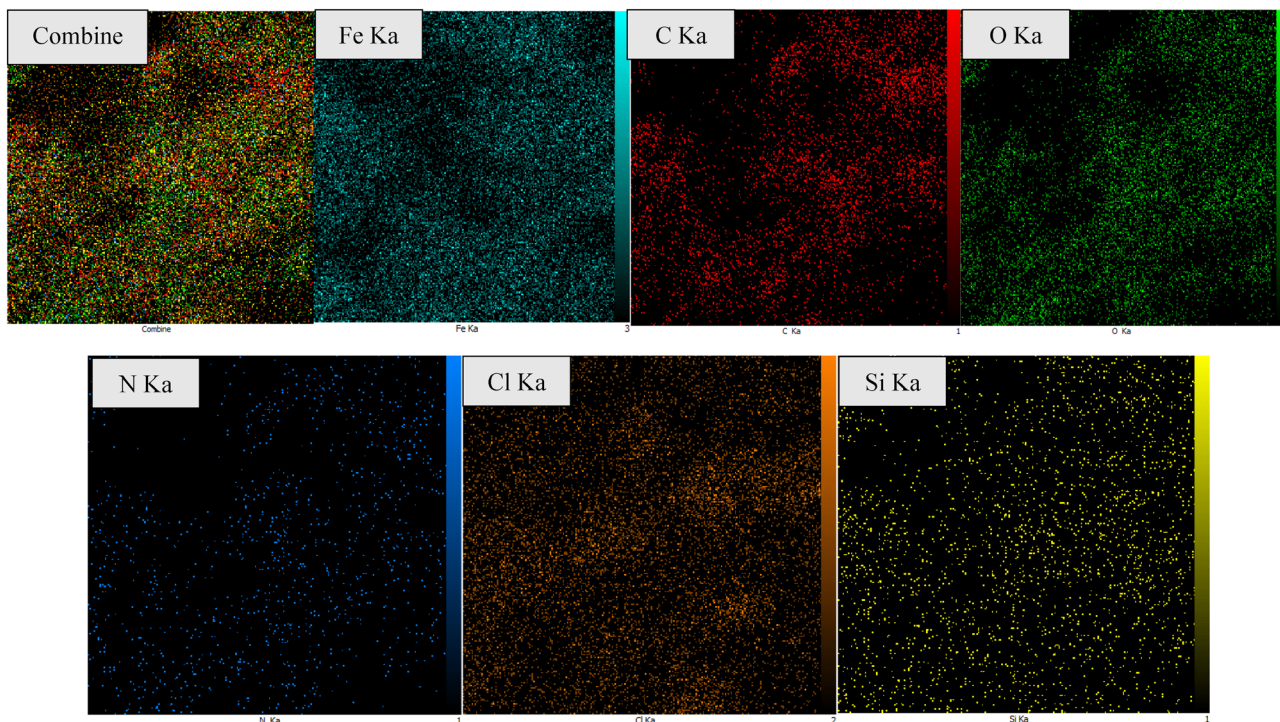


Figure 8. Maps of FNASiPPEA.

BET of FNASiPPEA. The BET (Brunauer–Emmett–Teller) surface area of the prepared nano-catalyst was obtained by nitrogen adsorption and desorption measurements (Fig. 9). The N_2 isotherms related to the type IV isotherm in the IUPAC classification have shown H_3 type rings, which can indicate the existence of mesopores and also have non-hard pores. As shown in Table 1 a, BJH (Barrett–Joyner–Halenda), and pore diameter were $7.0116 \text{ m}^2 \text{ g}^{-1}$, $0.050029 \text{ cm}^3 \text{ g}^{-1}$, and 28.206 nm respectively.

All the above results confirm the successful synthesis of magnetite biopolymer-based FNASiPPEA. After the detailed description of the prepared nano-catalyst, its catalytic performance was investigated for DHPC synthesis. Therefore, different reaction conditions such as the amount of catalyst, solvent, and temperature were investigated for a model reaction between 4-nitrobenzaldehyde, 4-hydroxycoumarin, and malononitrile (Table 2). While screening the model reaction in different solvents such as H_2O , EtOH, and $H_2O/EtOH$, the best result was obtained in the EtOH solvent (Table 2, entry 10).

After optimizing the reaction conditions, to determine the application range of FNASiPPEA, various aldehydes were used in the reaction. The results are summarized in Table 3.

Then, optimization of the reaction conditions for the synthesis of THBP was carried out. Hence, the reaction between 4-nitrobenzaldehyde, dimedone, and malononitrile in the presence of 0.02 g of catalyst at 50°C in solvent-free conditions has been adopted (Table 4, entry 9). The results are summarized in Table 4.

We used various aldehydes in the reaction to investigate the application range of FNASiPPEA as a magnetite biopolymer-based nano-catalyst. The result is presented in Table 5.

To compare the efficiency of this magnetite biopolymer-based nano-catalyst with other catalysts for the synthesis of DHPC and THBP derivatives, a summary of the results was collected in Tables 6 and 7. As can be seen in Tables 6 and 7, the reaction efficiency of this catalyst is better than other catalysts and the reaction time is shorter than others.

Hot filtration test. Because the FNASiPPEA is a heterogeneous nano-catalyst, a heterogeneity test called hot filtration was performed. In this way, first, the reaction was allowed to continue in the presence of the FNASiPPEA nano-catalyst, and then after half the time, the catalyst was removed from the reaction mixture and continued the reaction, as can be seen in Fig. 10a, no reaction progress was observed in the absence of the nano-catalyst, which indicates no leakage of solid catalyst into the reaction mixture. Therefore, the FNASiPPEA nano-catalyst is heterogeneous and suitable for DHPC and THBP synthesis reactions without any leaching.

Reusability of FNASiPPEA. To check the recyclability of the catalyst, after the completion of the reaction, the catalyst can be separated from the reaction mixture with a magnet, and after washing with chloroform ($CHCl_3$) and drying at the ambient temperature, and then can be reused for the synthesis of DHPC and THBP, which includes aldehyde (1 mmol), 1,3-diketone (4-hydroxycoumarin, dimedone), (1 mmol), and malononitrile (1.5 mmol) under optimized conditions. Therefore, the reusability of the catalyst for the model reaction was evaluated for the synthesis of DHPC and THBP (Figs. 11 and 12). FT-IR, XRD, VSM, and FESEM analyses of the nano-catalyst recovered after the 3rd run was also performed. According to Figs. 10b, c, d, and e, the matching

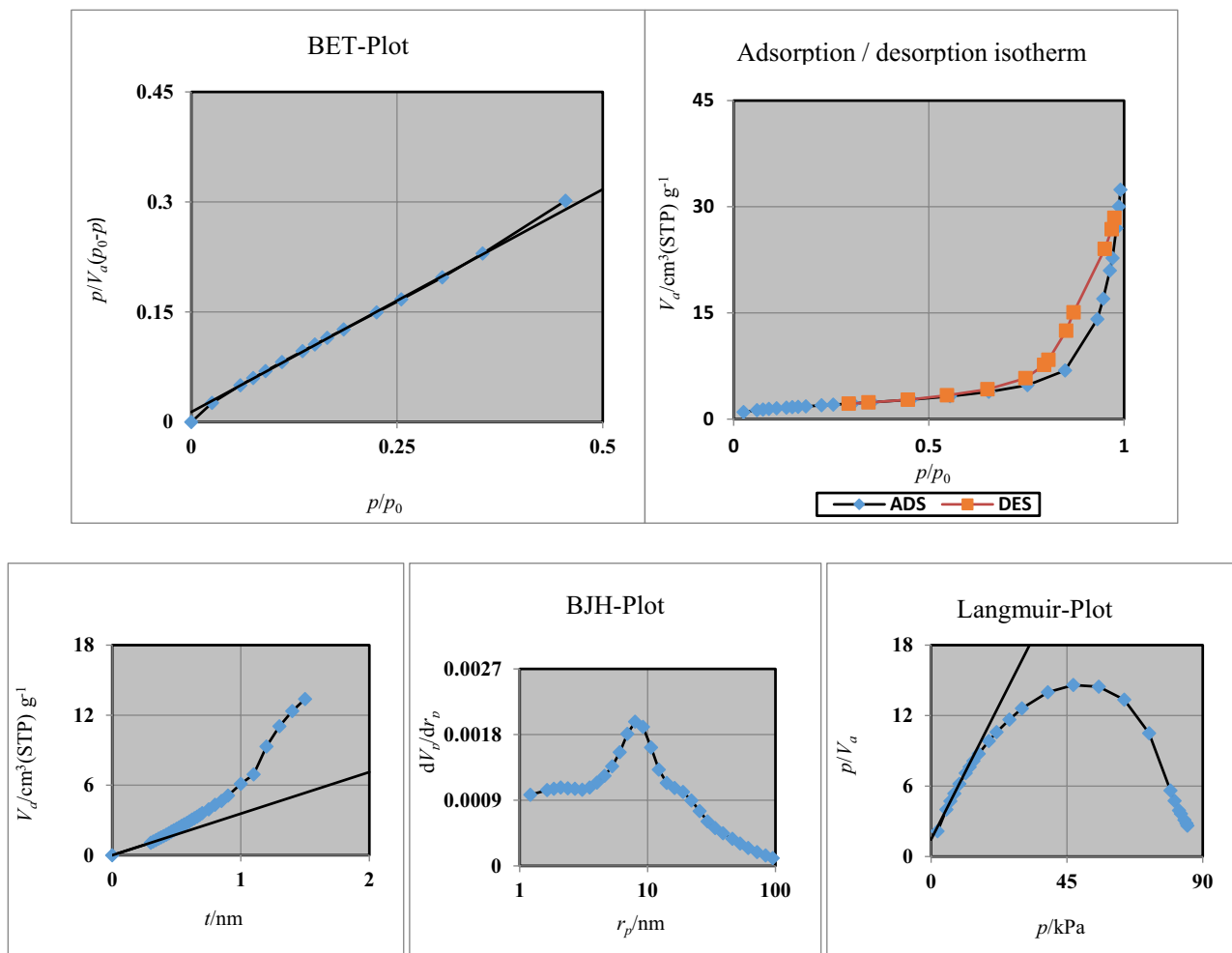
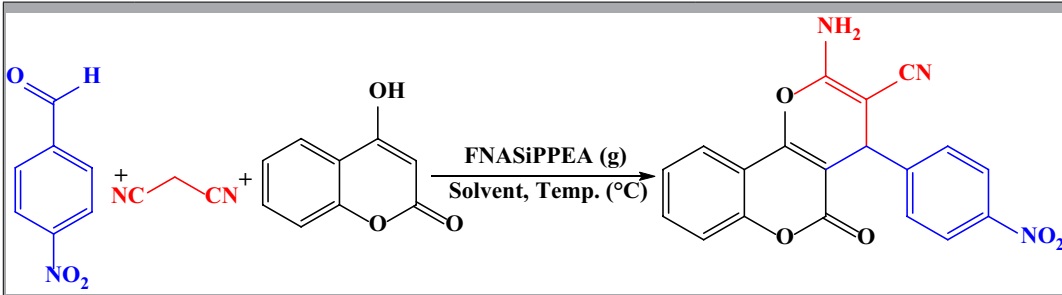


Figure 9. N₂ adsorption (blue line)—desorption (red line) isotherm and corresponding diagrams pore size distributions (BJH, BET, Langmuir, *t*-plot).

BET	
V_m	1.611 [cm ³ (STP) g ⁻¹]
$a_{s,BET}$	7.0116 [m ² g ⁻¹]
C	45.307
Total pore volume($p/p_0 = 0.990$)	0.049443 [cm ³ g ⁻¹]
Mean pore diameter	28.206 [nm]
Langmuir plot	
V_m	1.9705[cm ³ (STP) g ⁻¹]
$a_{s,Lang}$	7.0116 [m ² g ⁻¹]
B	0.3498
<i>t</i> plot	
Plot data	Adsorption branch
a_1	5.4877 [m ² g ⁻¹]
V_1	0 [cm ³ g ⁻¹]
BJH plot	
Plot data	Adsorption branch
V_p	0.050029 [cm ³ g ⁻¹]
$r_{p,peak}(Area)$	7.99 [nm]
a_p	9.0803 [m ² g ⁻¹]

Table 1. Parameters obtained from porosity analysis.



Entry	Conditions		
	Solvent/ Temp. (°C)/ Catalyst (g)	Time (min)	Yield (%) ^b
1	-/ r. t./ FNASiPPEA (0.005)	240	80
2	-/ r. t./ FNASiPPEA (0.01)	150	83
3	-/ r. t./ FNASiPPEA (0.015)	100	82
4	-/ r. t./ FNASiPPEA (0.02)	80	86
5	-/ 35/ FNASiPPEA (0.02)	80	85
6	-/ 45/ FNASiPPEA (0.02)	45	87
7	-/ 55/ FNASiPPEA (0.02)	40	86
8	-/ 65/ FNASiPPEA (0.02)	30	87
9	-/ 80/ FNASiPPEA (0.02)	30	89
10	EtOH/ 80/ FNASiPPEA (0.02)	10	95
11	EtOH: H ₂ O (1:1)/ 80/ FNASiPPEA (0.02)	25	95
12	H ₂ O/ 80/ FNASiPPEA (0.02)	30	90

Table 2. Optimization of reaction conditions for the synthesis of DHPC.^a Conditions: 4-nitrobenzaldehyde (1 mmol), 4-hydroxycoumarin (1 mmol), and malononitrile (1.5 mmol), Solvent (10 ml). ^bIsolated Yield.

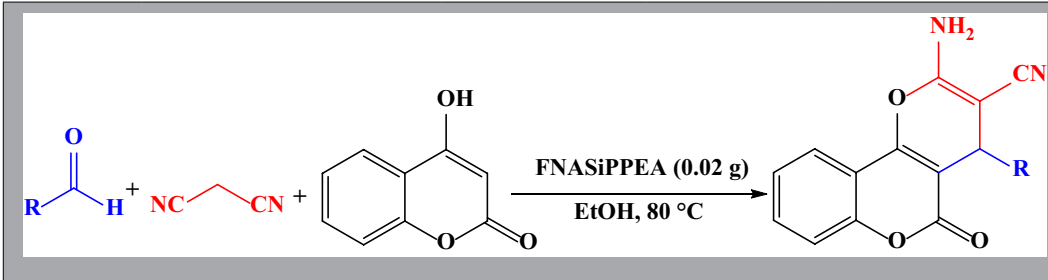
of FT-IR, XRD, VSM, and SEM patterns obtained after the third run with the primary nano-catalyst confirmed the preservation of the catalyst structure.

Proposed mechanism for synthesis of dihydropyrano[3,2-*c*]chromene and tetrahydrobenzo[*b*]pyran. Figure 13 shows the possible mechanism for the synthesis of dihydropyrano[3,2-*c*]chromene and tetrahydrobenzo[*b*]pyran derivatives using FNASiPPEA as a magnetite Brønsted base nano-catalyst. First, the Knoevenagel condensation between malononitrile and aldehyde is followed by loss of water to form an intermediate (a). Then the Michael addition between the intermediates (a) and (b) (dimedone, 4-hydroxycoumarin) and then intramolecular cyclization and tautomerization in the presence of the catalyst leads to the production of the corresponding product.

Experimental section

Materials and methods. Chemicals were purchased from Merck, Fluka, and Aldrich Chemical Companies. ¹H NMR and ¹³C NMR spectra were recorded at 400 and 100 MHz, respectively. Fourier transform infrared (FT-IR) measurements (in KBr pellets or ATR) were recorded on a Bruker spectrometer. Melting points were determined on a Büchi B-540 apparatus. The X-ray diffraction (XRD) pattern was obtained by a Philips Xpert MPD diffractometer equipped with a Cu K α anode ($k = 1.54 \text{ \AA}$) in the 2θ range from 10° to 80° . Field Emission Scanning Electron Microscopy (FESEM) was obtained on a Mira 3-XMU. VSM measurements were performed by using a vibrating sample magnetometer (Meghnatis Daghigh Kavir Co. Kashan Kavir, Iran). Energy-dispersive X-ray spectroscopy (EDS) of nano-catalyst was measured by an EDS instrument and Phenom pro X. The EDX-MAP micrographs were obtained on the MIRA II detector SAMX (France). Thermal gravimetric analysis (TGA) was conducted using the “STA 504” instrument. Transmission electron microscopy (TEM) was obtained using a Philips CM120 with a LaB6 cathode and an accelerating voltage of 120 kV. BELSORP MINI II nitrogen adsorption apparatus (Japan) for recording Brunauer–Emmett–Teller (BET) of nano-catalyst at 77 K.

Preparation of nano-almondshell. To prepare the nano-almondshell, the almondshell was heated in boiling water for 30 min, dried, and powdered. After that, was treated with a 17.5 w/v NaOH solution at 90°C for 24 h under reflux conditions. Subsequently, the almondshell was filtered and washed with distilled water until the alkali was eliminated. Then, bleached with 100 mL of 1:1 aqueous dilution of 3.5% w/v sodium hypochlorite (NaOCl) at 80°C for 3 h under reflux conditions. The resulting almondshell particles were hydrolyzed partially using the 35% sulfuric acid (H₂SO₄) aqueous solution with an almondshell-to-acid weight ratio of 1–10 at 45°C . After 3 h, the obtained suspension was diluted with water five-fold to stop the hydrolysis reaction. The suspension was centrifuged at 4000 rpm to separate the nano-almondshell from the acidic medium (yield 60%).



Entry	R	Time (min)	Yield (%) ^b	m. p. (refs.)
1	4-NO ₂ -C ₆ H ₄ -	5	95	259–261 ⁴⁴
2	4-F-C ₆ H ₄ -	7	96	261–263 ⁴⁵
3	4-Br-C ₆ H ₄ -	5	96	248–250 ⁴⁴
4	4-OH-C ₆ H ₄ -	10	94	260–262 ⁴⁴
5	4-OMe-C ₆ H ₄ -	15	94	248–251 ⁴⁶
6	4-isopropyl-C ₆ H ₄ -	25	90	250–252 ⁴⁵
7	3-NO ₂ -C ₆ H ₄ -	30	93	261–263 ⁴⁴
8	2-NO ₂ -C ₆ H ₄ -	30	95	259–261 ⁴⁴
9	2-Cl-C ₆ H ₄ -	35	95	273–275 ⁴⁵
10	2,4-(Cl) ₂ -C ₆ H ₃ -	10	98	259–261 ⁴⁶
11	2,6-(Cl) ₂ -C ₆ H ₃ -	20	90	273–276 ⁴⁷
12	C ₆ H ₅ -	20	92	255–257 ⁴⁶
13	3-pyridine-	5	96	250–252
14	Pentyl-	25	80	188–190 ⁴⁸

Table 3. FNASiPPEA catalyzed the synthesis of DHPC.^a ^aConditions: aldehyde (1 mmol), 4-hydroxycoumarin (1 mmol), malononitrile (1.5 mmol), 80 °C, EtOH Solvent, catalyst (0.02 g) ^bIsolated yield.

Preparation of Fe₃O₄@nano-almondshell. In a 250 mL flask, 3 g of nano-almondshell and 100 mL acetic acid (CH₃COOH) of 0.05 M were added. After that, FeCl₃·6H₂O (3.51 g, 13 mmol) and FeCl₂·4H₂O (1.29 g, 6.5 mmol) were added and stirred for 6 h at 80 °C. Then, 8 mL of NH₄OH (25%), was added dropwise and stirred for 45 min. The precipitated brown products were isolated from the solution by a magnet, washed 3 times with distilled water, and dried in an oven at 80 °C for 4 h. The weight of the Fe₃O₄@nano-almondshell obtained is 4.141 g.

Synthesis of Fe₃O₄@nano-almondshell/Si(CH₂)₃Cl (FNASiP-Cl). In a 100 mL flask, 1 g of dried Fe₃O₄@nano-almondshell was dispersed in the mixture of 10 mL of chloroform (CHCl₃), and 3.4 mL of 3-chloropropyltrimethoxysilane was added dropwise. The mixture was sonicated at 25 °C for 20 min and then, the mixture was carried out under reflux conditions for 4 h. Finally, the result was collected using a magnet and washed three times with chloroform.

Preparation of magnetite FNASiPPEA. The FNASiP-Cl (0.5 g) was dispersed in ethanol by ultrasonic for 20 min at room temperature and then dried. The next, 0.5 g of dried FNASiP-Cl and 2-(1-piperazinyl)ethylamine (AEP) (0.129 g, 1 mmol) was heated in 10 mL *N,N*-dimethylformamide (DMF) for 24 h at 80 °C. The resulting precipitates were cooled, washed with dichloromethane (CH₂Cl₂), and dried.

General synthesis of dihydropyrano[3,2-*c*]chromene and tetrahydrobenzo[*b*]pyran derivatives. For the synthesis of dihydropyrano[3,2-*c*]chromene, in a 50 mL round bottom flask, 4-hydroxycoumarin (1 mmol, 0.162 g), 4-nitrobenzaldehyde (1 mmol, 0.151 g), malononitrile (1.5 mmol, 0.099 g), FNASiPPEA (0.02 g), and 10 mL EtOH was added. The reaction mixture was refluxed at 80 °C and stirred for appropriate periods as shown in Table 2. After the end of the reaction (TLC, *n*-hexane: ethyl acetate 6:4), the catalyst FNASiPPEA was separated from the reaction mixture by an external magnet, the solvent was removed under reduced pressure, and the precipitate was washed with methanol and recrystallized with chloroform for further purification.

Entry	Conditions		
	Solvent/ Temp. (°C)/ Catalyst (g)	Time (min)	Yield (%) ^b
1	-/ r. t./ FNASiPPEA (0.01)	110	83
2	-/ r. t./ FNASiPPEA (0.015)	88	82
3	-/ r. t. / FNASiPPEA (0.02)	75	86
4	-/ 35/ FNASiPPEA (0.02)	60	85
5	-/ 45/ FNASiPPEA (0.02)	45	87
6	-/ 50/ FNASiPPEA (0.02)	20	88
7	-/ 55/ FNASiPPEA (0.02)	30	86
8	-/ 80/ FNASiPPEA (0.02)	80	89
9	EtOH/ 50/ FNASiPPEA (0.02)	5	95
10	EtOH: H ₂ O (1:1)/ 50/ FNASiPPEA (0.02)	25	95
11	H ₂ O/ 50/ FNASiPPEA (0.02)	30	90

Table 4. Optimization of the reaction conditions for the synthesis of THBP.^a ^aconditions: 4-nitrobenzaldehyde (1 mmol), dimesone (1 mmol), malononitrile (1.5 mmol), Solvent (10 ml). ^bIsolated Yield.

Entry	R	Time (min)	Yield (%) ^b	m. p. (refs.)
1	4-NO ₂ -C ₆ H ₄ -	5	95	181–217 ⁴⁹
2	4-F-C ₆ H ₄ -	5	94	191–194 ⁴⁹
3	4-Br-C ₆ H ₄ -	5	96	199–200 ⁴⁹
4	4-Cl-C ₆ H ₄ -	7	97	215–216 ⁴⁸
5	4-OH-C ₆ H ₄ -	15	94	213–215 ⁵¹
6	4-OMe-C ₆ H ₄ -	15	94	208–210 ⁵¹
8	3-NO ₂ -C ₆ H ₄ -	35	93	216–218 ⁵¹
9	2-NO ₂ -C ₆ H ₄ -	35	95	234–236 ⁵¹
10	2-Cl-C ₆ H ₄ -	35	95	216–218 ⁵⁰
11	2,6-(Cl) ₂ -C ₆ H ₃ -	15	95	249–251 ⁵¹
12	C ₆ H ₅ -	25	92	231–234 ⁵¹
13	Furan-	15	94	217–219 ⁵¹
14	Pentyl-	30	83	162–164 ⁵¹
15	Styryl-	25	90	217–219 ⁵¹

Table 5. Synthesis of THBP derivatives catalyzed by FNASiPPEA.^a ^aConditithons: aldehyde (1 mmol), dimesone (1 mmol), malononitrile (1.5 mmol), 50 °C, EtOH as the solvent, catalyst (0.02 g), ^bIsolated yield.

Entry	Conditions			
	Temp. (°C), Solvent, Catalyst	Time (min)	Yield (%)	Refs
1	70, H ₂ O: EtOH, MNPs-PhSO ₃ H	15	87	⁵²
2	90, Solvent-free, Fe ₃ O ₄ @SiO ₂ -Imine/Phenoxy-Cu(II)	17	95	⁵³
3	80, Solvent-free, f CoFe ₂ O ₄ @FA-Er	26	96	⁵⁴
4	Reflux, EtOH, Zn ₃ (PO ₄) ₂ ·4H ₂ O	30	85	⁵⁵
5	80, EtOH, FNASiPPEA	10	95	This work

Table 6. Comparison of FNASiPPEA with other catalysts for the synthesis of DHPC.

Entry	Conditions			
	Temp. (°C), Solvent, Catalyst	Time (min)	Yield (%)	Refs
1	80, EtOH, NH ₄ Al(SO ₄) ₂ ·12H ₂ O	130	93	⁵⁶
2	r. t., H ₂ O, (S)-proline	30	82	⁵⁷
3	50, EtOH, Hal-Py-IL	90	100	⁵⁸
4	100, H ₂ O, ChCl/urea/thiourea DES	17	90	⁵⁹
5	50, EtOH, FNASiPPEA	5	95	This work

Table 7. Comparison activity of FNASiPPEA with another catalyst for the synthesis of THBP.

For the synthesis of tetrahydrobenzo[*b*]pyran, the reaction of dimedone (1 mmol, 0.140 g), 4-nitrobenzaldehyde (1 mmol, 0.151 g), malononitrile (1.5 mmol, 0.099 g), and magnetite nano-catalyst FNASiPPEA (0.02 g) was carried out in 10 ml of EtOH (Table 4). After the completion of the reaction (TLC, *n*-hexane: ethyl acetate 7:3), the magnetite catalyst was removed from the reaction mixture by a magnet, the solvent was removed under reduced pressure, and the product was obtained after washing and recrystallization with chloroform.

Conclusion

In summary, the magnetite almondshell-based nano-catalyst was prepared, characterized, and used for the synthesis of DHPC and THBP. The prepared nano-catalyst FNASiPPEA shows high catalytic activity and good reusability. Meanwhile, this method is non-toxic and biodegradable, it may be used to prepare other biopolymer-based nano-catalysts for more interesting reactions.

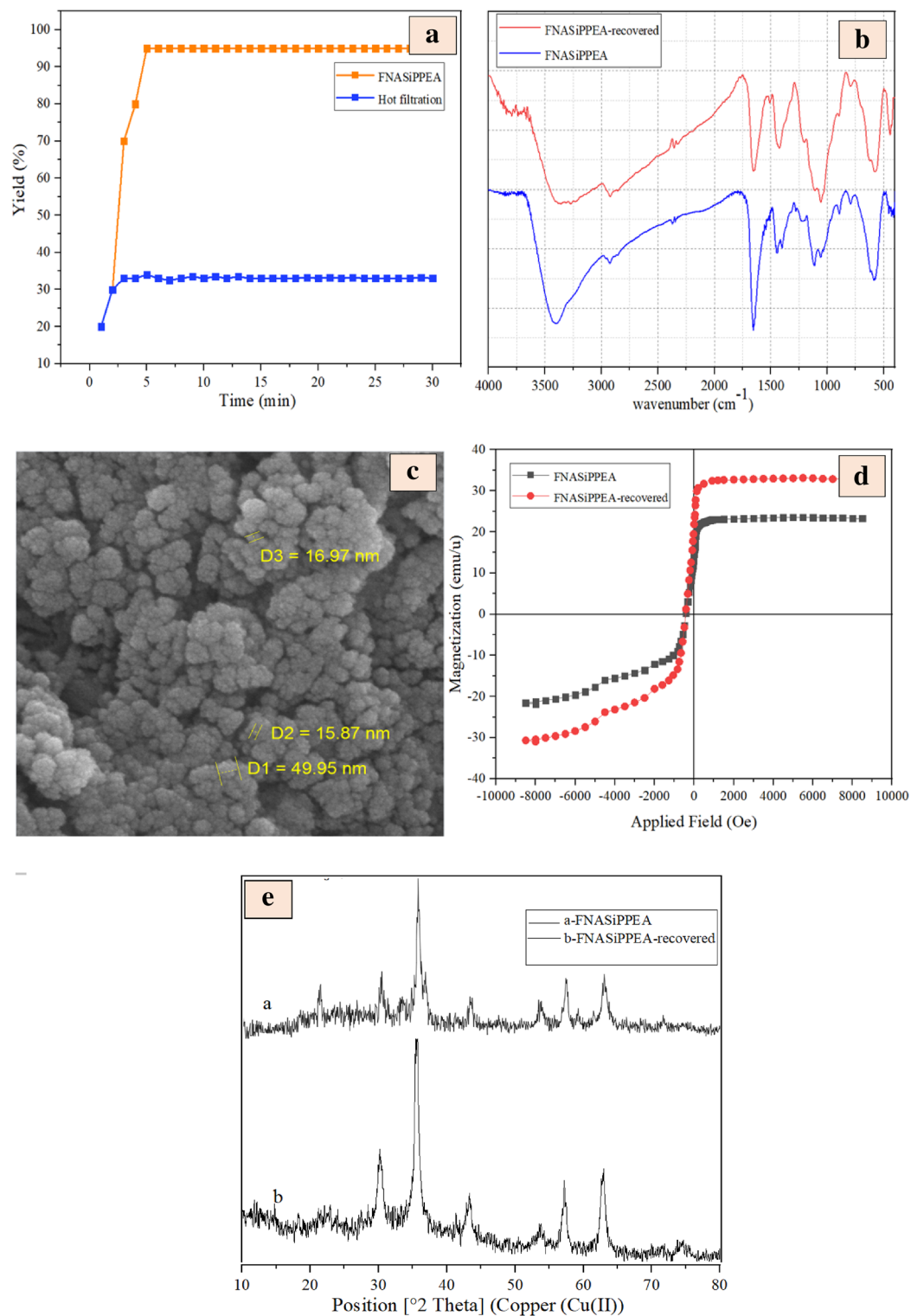


Figure 10. (a) Hot filtration test, (b) FT-IR, (c) FESEM, (d) VSM, and (e) XRD of recovered bio-based nano-catalyst.

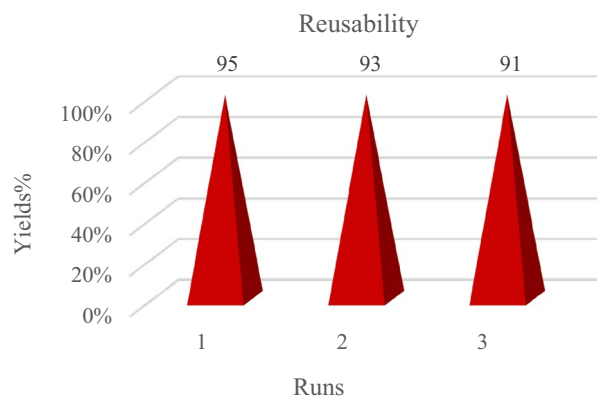


Figure 11. Reusability of FNASiPPEA for the synthesis of DHPC.

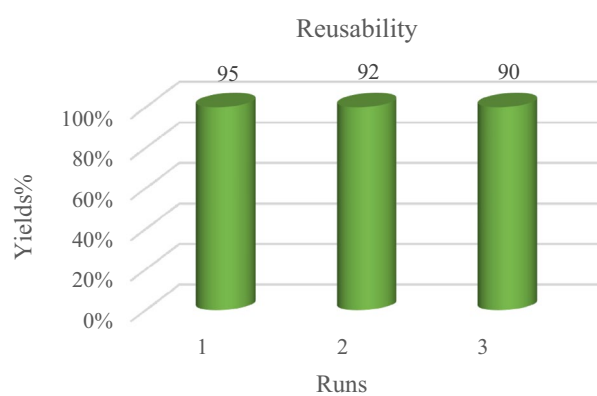


Figure 12. Recyclability of FNASiPPEA for the synthesis of THBP.

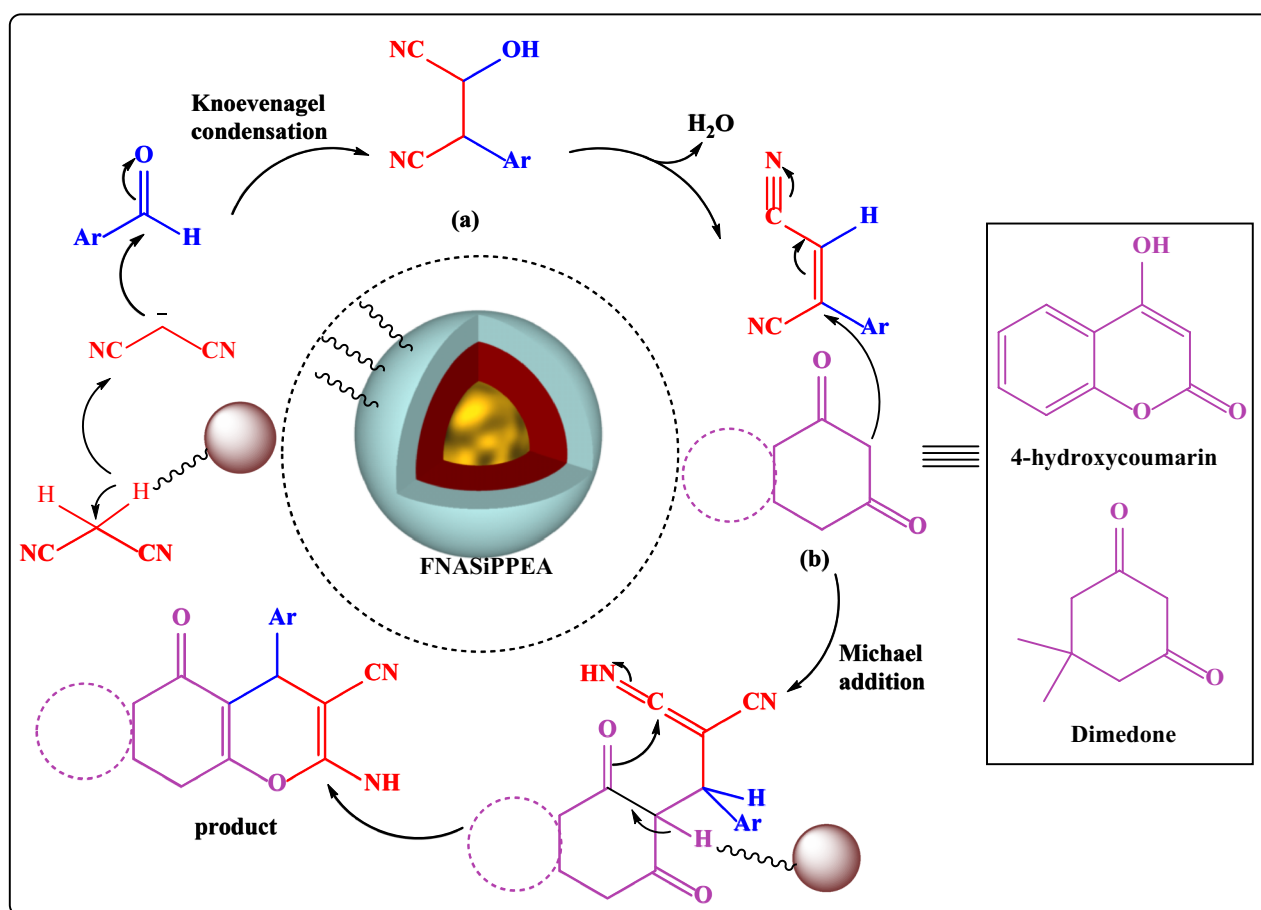


Figure 13. Proposed mechanism for synthesis of DHPC and THBP.

Data availability

The datasets generated and/or analysed during the current study are available in this article and its supplementary information files.

Received: 26 October 2022; Accepted: 11 April 2023

Published online: 19 April 2023

References

- Li, C. *et al.* Fiber-based biopolymer processing as a route toward sustainability. *Adv. Mater.* **34**(1), 2105196 (2022).
- Apriyanto, A., Compart, J. & Fettke, J. A review of starch, a unique biopolymer—structure, metabolism and in planta modifications. *Plant Sci.* 111223 (2022).
- Baranwal, J., Barse, B., Fais, A., Delogu, G. L. & Kumar, A. Biopolymer: A sustainable material for food and medical applications. *Polymers* **14**(5), 983 (2022).
- Balart, R., Garcia-Garcia, D., Fombuena, V., Quiles-Carrillo, L. & Arrieta, M. P. Biopolymers from natural resources. *Polymers* **13**(15), 2532 (2021).
- Kargarzadeh, H. *et al.* Advances in cellulose nanomaterials. *Cellulose* **25**(4), 2151–2189 (2018).
- Foster, E. J. *et al.* Current characterization methods for cellulose nanomaterials. *Chem. Soc. Rev.* **47**(8), 2609–2679 (2018).
- Rol, F., Belgacem, M. N., Gandini, A. & Bras, J. Recent advances in surface-modified cellulose nanofibrils. *Prog. Polym. Sci.* **88**, 241–264 (2019).
- Seddiqi, H. *et al.* Cellulose and its derivatives: Towards biomedical applications. *Cellulose* **28**(4), 1893–1931 (2021).
- Javadi, T., Mahmood, S., Saeed, W. & Qamrosh, M. A critical review in varieties and benefits of almond (*Prunus dulcis*). *Act. Sci. Nutr. Health* **3**(11), 70–72 (2019).
- Li, X., Liu, Y., Hao, J. & Wang, W. Study of almond shell characteristics. *Materials* **11**(9), 1782 (2018).
- Ebringerová, A., Hromádková, Z., Zuzana, K. & Sasínková, V. Chemical valorization of agricultural by-products: Isolation and characterization of xylan-based antioxidants from almond shell biomass. *BioResources* **3**(1), 60–70 (2007).
- Senturk, H. B., Ozdes, D. & Duran, C. Biosorption of Rhodamine 6G from aqueous solutions onto almond shell (*Prunus dulcis*) as a low cost biosorbent. *Desalination* **252**(1–3), 81–87 (2010).
- Mohan, D., Sarswat, A., Singh, V. K., Alexandre-Franco, M. & Pittman, C. U. Development of magnetic activated carbon from almond shells for trinitrophenol removal from water. *Chem. Eng. J.* **172**(2–3), 1111–1125 (2011).
- Mallah, D. & Mirjalili, B. F. FNAOSiPPEA/Zn(II) as a bifunctional Lewis acid/Bronsted base heterogeneous magnetic nanocatalyst based on nano-almond shell for synthesis of naphtho [1, 3] oxazine derivatives. *ChemistrySelect* **6**(42), 1483–11489 (2021).
- Mallah, D. & Mirjalili, B. F. Preparation and application of FNAOSiPPEA/Cu (II) as a novel magnetite almondshell based Lewis acid-Bronsted base nano-catalyst for the synthesis of pyrimidobenzothiazoles. *BMC Chem.* **16**(1), 1–13 (2022).

16. Chaudhary, A. *et al.* Chromenes—a novel class of heterocyclic compounds: Recent advancements and future directions. *Mini Rev. Med. Chem.* **22**(21), 2736–2751 (2022).
17. Pratap, R. & Ram, V. J. Natural and synthetic chromenes, fused chromenes, and versatility of dihydrobenzo [*h*] chromenes in organic synthesis. *Chem. Rev.* **114**(20), 10476–10526 (2014).
18. Katiyar, M. K., Dhakad, G. K., Arora, S., Bhagat, S., Katyal, T. & Kumar, R. Synthetic strategies and pharmacological activities of chromene and its derivatives: an overview. *J. Mol. Struct.* 133012 (2022).
19. Khafagy, M. M., El-Wahas, A. H. F. A., Eid, F. A. & El-Agrody, A. M. Synthesis of halogen derivatives of benzo[*h*]chromene and benzo[*a*]anthracene with promising antimicrobial activities. *Farmaco* **57**(9), 715–722 (2002).
20. Nawaz, M., Abbasi, M. W. & Hisaindee, S. Synthesis, characterization, anti-bacterial, anti-fungal and nematocidal activities of 2-amino-3-cyanochromenes. *J. Photochem. Photobiol. B: Biol.* **164**, 160–163 (2016).
21. Gourdeau, H. *et al.* Antivascular and antitumor evaluation of 2-amino-4-(3-bromo-4, 5-dimethoxy-phenyl)-3-cyano-4-*H*-chromenes, a novel series of anticancer agents. *Mol. Cancer Ther.* **3**(11), 1375–1384 (2004).
22. Denish, C. K., Hetal, K. P. & Nilesh, K. G. Synthesis, characterization & anti-HIV activity of 4-hydroxy-3-(5-methylisoxazol-3-yl)pyrano (3, 2-*C*) chromene-2, 5-dione. *AJBPR* **2**(2), 126–130 (2012).
23. Bianchi, G. & Tava, A. Synthesis of (2*R*)-(+)-2, 3-dihydro-2, 6-dimethyl-4-*H*-pyran-4-one, a homologue of pheromones of a species in the hepialidae family. *Agric. Biol. Chem.* **51**(7), 2001–2002 (1987).
24. Laskar, S. & Brahmachari, G. Access to biologically relevant diverse chromene heterocycles via multicomponent reactions (MCRs): Recent advances. *Org. Biomol. Chem.* **2**, 1–50 (2014).
25. Mamaghani, M., Nia, R. H., Tavakoli, F. & Jahanshahi, P. Recent advances in the MCRs synthesis of chromenes: A review. *Curr. Org. Chem.* **22**(17), 1704–1769 (2018).
26. Saranya, S., Aneja, T., Neetha, M. & Anilkumar, G. Recent advances in the iron-catalysed multicomponent reactions. *Appl. Organomet. Chem.* **34**(12), e5991 (2020).
27. Darvishy, S., Alinezhad, H., Vafaezadeh, M., Peiman, S. & Maleki, B. S-(+) Camphorsulfonic acid glycine (csag) as surfactant-like Brønsted acidic ionic liquid for one-pot synthesis of β-amino carbonyl. *Polycycl. Aromat. Compd.* 1–13 (2022).
28. Karbasaki, S. S., Bagherzade, G., Maleki, B. & Ghani, M. Magnetic Fe₃O₄@ SiO₂ core-shell nanoparticles functionalized with sulfamic acid polyamidoamine (pamam) dendrimer for the multicomponent synthesis of polyhydroquinolines and dihydro-1*H*-indeno [1, 2-*b*] pyridines. *Org. Prep. Proced. Int.* **53**(5), 498–508 (2021).
29. Chen, M. N., Mo, L. P., Cui, Z. S. & Zhang, Z. H. Magnetic nanocatalysts: synthesis and application in multicomponent reactions. *Curr. Opin. Green Sustain. Chem.* **15**, 27–37 (2019).
30. Saha, A., Payra, S. & Banerjee, S. On water synthesis of pyran–chromenes via a multicomponent reactions catalyzed by fluorescent t-ZrO₂ nanoparticles. *RSC Adv.* **5**(123), 101664–101671 (2015).
31. Banerjee, S. & Saha, A. Free-ZnO nanoparticles: A mild, efficient and reusable catalyst for the one-pot multicomponent synthesis of tetrahydrobenzo [*b*] pyran and dihydropyrimidone derivatives. *New J. Chem.* **37**(12), 4170–4175 (2013).
32. Jarrahi, M., Maleki, B. & Tayeb, R. Magnetic nanoparticle-supported eosin Y salt [SB-DABCO@eosin] as an efficient heterogeneous photocatalyst for the multi-component synthesis of chromeno [4, 3-*b*] chromene in the presence of visible light. *RSC Adv.* **12**(45), 28886–28901 (2022).
33. Boroumand, H., Alinezhad, H., Maleki, B. & Peiman, S. Triethylenetetramine-grafted magnetic graphene oxide (Fe₃O₄@ GO-NH₂) as a reusable heterogeneous catalyst for the one-pot synthesis of 2-amino-4*H*-benzopyran derivatives. *Polycycl. Aromat. Compd.* (2022), In press.
34. Patil, P., Kadam, S., Patil, D. & More, P. An eco-friendly innovative halide and metal-free basic ionic liquid catalyzed synthesis of tetrahydrobenzo [*b*] pyran derivatives in aqueous media: A sustainable protocol. *J. Mol. Liq.* **345**, 117867 (2022).
35. Kataraya, A. P. *et al.* An efficient and green synthesis of tetrahydrobenzo [*b*] pyran derivatives using [(EMIM) Ac] at room temperature. *ChemistrySelect* **7**(15), e202104184 (2022).
36. Kate, P., Pandit, V., Jawale, V. & Bachute, M. L-Proline catalyzed one-pot three-component synthesis and evaluation for biological activities of tetrahydrobenzo [*b*] pyran: Evaluation by green chemistry metrics. *J. Chem. Sci.* **134**, 1–11 (2022).
37. Nesaragi, A. R. *et al.* Chitosan-ZnO: An efficient and recyclable polymer incorporated hybrid nanocatalyst to synthesize tetrahydrobenzo [*b*] pyrans and pyrano [2,3-*d*] pyrimidinones under microwave expedition. *ChemistrySelect* **7**(14), e202200604 (2022).
38. Patil, S. P., Shinde, S. K., Patil, M. U. & Patil, S. S. Coconut endocarp shell ash (CESA): a versatile and waste-originated catalyst for the synthesis of tetrahydrobenzo [*b*] pyrans and 1, 4-dihydropyridines. *Res. Chem. Intermed.* **48**(8), 3589–3612 (2022).
39. Banerjee, B. *et al.* Glycine catalyzed one-pot three-component synthesis of structurally diverse 2-amino substituted pyran annulated heterocycles in aqueous ethanol under refluxed conditions. *Curr. Green Chem.* **9**(3), 162–173 (2022).
40. Bayzidi, M. & Zeynizadeh, B. The immobilized zirconocene chloride on magnetite-reduced graphene oxide: A highly efficient and reusable heterogeneous nanocatalyst for one-pot three-component synthesis of tetrahydrobenzo [*b*] pyrans and dihydropyran [3, 2-*c*] chromenes. *ChemistrySelect* **7**(43), e202202708 (2022).
41. Xu, L. *et al.* Green synthesis of Cu/Fe₃O₄ nanoparticles using green tea extract: Evaluation of its catalytic activity, antioxidant and anti-colon cancer effects. *Inorg. Chem. Commun.* **144**, 109927 (2022).
42. Azi, S. & Mirjalili, B. F. TiCl₄/nano-cellulose: A biodegradable and eco-friendly bio-based catalyst for one-pot synthesis of 4*H*-pyrimido [2,1-*b*] benzothiazole derivatives. *RSC Adv.* **6**, 96928–96934 (2016).
43. Chicea, D., Indrea, E. & Cretu, C. M. Assessing Fe₃O₄ nanoparticle size by DLS, XRD and AFM. *J. Optoelectron. Adv. Mater.* **14**(5), 460 (2012).
44. Niknam, K. & Jamali, A. Silica-bonded N-propylpiperazine sodium *n*-propionate as recyclable basic catalyst for synthesis of 3,4-dihydropyran [c] chromene derivatives and biscoumarins. *Chinese J. Catal.* **33**(11–12), 1840–1849 (2012).
45. Khurana, J. M., Nand, B. & Saluja, P. DBU: A highly efficient catalyst for one-pot synthesis of substituted 3, 4-dihydropyran [3, 2-*c*] chromenes, dihydropyran [4, 3-*b*] pyranes, 2-amino-4*H*-benzo [*h*] chromenes and 2-amino-4*H* benzo [*g*] chromenes in aqueous medium. *Tetrahedron* **66**(30), 5637–5641 (2010).
46. Ghashang, M., Mansoor, S. S., Shams Solaree, L. & Sharifian-esfahani, A. Multi-component, one-pot, aqueous media preparation of dihydropyran [3, 2-*c*] chromene derivatives over MgO nanoplates as an efficient catalyst. *Iran. J. Catal.* **6**(3), 237–243 (2016).
47. Ghorbani-Vaghei, R., Toghræi-Semiromi, Z. & Karimi-Nami, R. One-pot synthesis of 4*H*-chromene and dihydropyran [3, 2-*c*] chromene derivatives in hydroalcoholic media. *J. Braz. Chem. Soc.* **22**, 905–909 (2011).
48. Khazdooz, L. *et al.* Highly efficient and environmentally benign method for the synthesis of tetrahydrobenzo[*b*]pyrans using Ca₉Mg_{0.5}(PO₄)_{5.5}(SiO₄)_{0.5}F_{1.5} as a new bio- and nanocatalyst with Brønsted base and Lewis acid properties. *Res. Chem. Intermed.* **44**(1), 93–115 (2018).
49. Maleki, B., Nasiri, N., Tayeb, R., Khojastehnezhad, A. & Akhlaghi, H. A. Green synthesis of tetrahydrobenzo[*b*]pyrans, pyrano[2,3-*c*]pyrazoles and spiro[indoline-3,4'-pyrano[2,3-*c*]pyrazoles catalyzed by nano-structured diphosphate in water. *RSC Adv.* **6**(82), 79128–79134 (2016).
50. Hasaninejad, A., Golzar, N., Beyrati, M., Zare, A. & Doroodmand, M. M. Silica-bonded 5-*n*-propyl-octahydro-pyrimido[1,2-*a*]azepinium chloride (SB-DBU) Cl as a highly efficient, heterogeneous and recyclable silica-supported ionic liquid catalyst for the synthesis of benzo[*b*]pyran, bis(benzo[*b*]pyran) and spiro-pyran derivatives. *J. Mol. Catal. A: Chem.* **372**, 137–150 (2013).
51. Mehravar, M., Mirjalili, B. F., Babaei, E. & Bamoniri, A. Nano-SiO₂/DBN: an efficacious and reusable catalyst for one-pot synthesis of tetrahydrobenzo [*b*] pyran derivatives. *BMC Chem.* **15**(1), 1–10 (2021).

52. Faroughi Niya, H., Hazeri, N., Rezaie Kahkhaie, M. & Maghsoodlou, M. T. Preparation and characterization of MNPs-PhSO₃H as a heterogeneous catalyst for the synthesis of benzo [b] pyran and pyrano [3, 2-c] chromenes. *Res. Chem. Intermed.* **46**(3), 1685–1704 (2020).
53. Nesarvand, M., Azarifar, D. & Ebrahimiasl, H. One-pot and green synthesis 1*H*-pyrazolo [1, 2-*b*] phthalazine-5, 10-dione and dihydropyrano [3, 2-*c*] chromene derivatives by Fe₃O₄@ SiO₂-imine/phenoxy-Cu (II) as an efficient and reusable catalyst. *Res. Chem. Intermed.* **47**(9), 3629–3644 (2021).
54. Sorkhabi, S., Mozafari, R. & Ghadermazi, M. New advances in catalytic performance of erbium-folic acid-coated CoFe₂O₄ complexes for green one-pot three-component synthesis of pyrano [2, 3-*d*] pyrimidinone and dihydropyrano [3, 2-*c*] chromenes compounds in water. *Appl. Organomet. Chem.* **35**(7), e6225 (2021).
55. Hallaoui, A. E. *et al.* Application of phosphate fertilizer modified by zinc as a reusable efficient heterogeneous catalyst for the synthesis of biscoumarins and dihydropyrano [3, 2-*c*] chromene-3-carbonitriles under green conditions. *Polycycl. Aromat. Compd.* **41**(10), 2083–2102 (2021).
56. Mohammadi, A. A., Asghariganjeh, M. R. & Hadadzahmatkesh, A. Synthesis of tetrahydrobenzo [b] pyran under catalysis of NH₄Al (SO₄)₂·12H₂O (Alum). *Arab. J. Chem.* **10**, S2213–S2216 (2017).
57. Balalaie, S., Bararjanian, M., Amani, A. M. & Movassagh, B. (S)-Proline as a neutral and efficient catalyst for the one-pot synthesis of tetrahydrobenzo [b] pyran derivatives in aqueous media. *Synlett* **2006**(02), 263–266 (2006).
58. Sadjadi, S., Koohestani, F., Abedian-Dehaghani, N. & Heravi, M. M. Halloysite nanoclay with high content of sulfonic acid-based ionic liquid: a novel catalyst for the synthesis of tetrahydrobenzo [b] pyrans. *Catal.* **11**(10), 1172 (2021).
59. Biglari, M., Shirini, F., Mahmoodi, N. O., Zabihzadeh, M. & Mashhadinezhad, M. A choline chloride-based deep eutectic solvent promoted three-component synthesis of tetrahydrobenzo [b] pyran and pyrano [2, 3-*d*] pyrimidinone (thione) derivatives. *J. Mol. Struct.* **1205**, 127652 (2020).

Acknowledgements

The authors would like to thank Yazd University, Yazd, Iran.

Author contributions

D.M. is a Ph.D. student. She has worked on the subject of manuscripts in the laboratory with A.H.B. and B.F.M. helps as a supervisor. D.M. wrote the manuscript, and A.H.B. and B.F.M. edit the manuscript.

Competing interests

The authors declare no competing interests.

Additional information

Supplementary Information The online version contains supplementary material available at <https://doi.org/10.1038/s41598-023-33286-w>.

Correspondence and requests for materials should be addressed to B.B.F.M.

Reprints and permissions information is available at www.nature.com/reprints.

Publisher's note Springer Nature remains neutral with regard to jurisdictional claims in published maps and institutional affiliations.



Open Access This article is licensed under a Creative Commons Attribution 4.0 International License, which permits use, sharing, adaptation, distribution and reproduction in any medium or format, as long as you give appropriate credit to the original author(s) and the source, provide a link to the Creative Commons licence, and indicate if changes were made. The images or other third party material in this article are included in the article's Creative Commons licence, unless indicated otherwise in a credit line to the material. If material is not included in the article's Creative Commons licence and your intended use is not permitted by statutory regulation or exceeds the permitted use, you will need to obtain permission directly from the copyright holder. To view a copy of this licence, visit <http://creativecommons.org/licenses/by/4.0/>.

© The Author(s) 2023